Crystal structure of Pseudomonas aeruginosa lipase in the open conformation - The prototype for family I.1 of bacterial lipases

Nardini, M; Lang, DA; Liebeton, K; Jaeger, KE; Dijkstra, BM

Published in:
The Journal of Biological Chemistry

DOI:
10.1074/jbc.M003903200

Publication date:
2000

THE JOURNAL OF BIOLOGICAL CHEMISTRY
Vol. 275, No. 40, Issue of October 6, pp. 31219–31225, 2000

Printed in U.S.A.

Crystal Structure of *Pseudomonas aeruginosa* Lipase in the Open Conformation

THE PROTOTYPE FOR FAMILY I.1 OF BACTERIAL LIPASES*

Received for publication, May 8, 2000, and in revised form, June 30, 2000
Published, JBC Papers in Press, July 12, 2000, DOI 10.1074/jbc.M003903200

Marco Nardini‡§¶, Dietmar A. Lang¶‖, Klaus Liebeton‡‡, Karl-Erich Jaeger‡‡, and Bauke W. Dijkstra‡§§**

From the ‡Laboratory of Biophysical Chemistry and BIOSON Research Institute, Department of Chemistry, University of Groningen, Nijenborgh 4, 9747 AG Groningen, The Netherlands, ‖EMBL, Hamburg Outstation, DESY, Notkestraβe 85, 22603 Hamburg, Germany, and ‡‡Lehrstuhl für Biologie der Mikroorganismen, Ruhr-Universität Bochum, Universitätsstraβe 150, 44780 Bochum, Germany

The x-ray structure of the lipase from *Pseudomonas aeruginosa* PAO1 has been determined at 2.54 Å resolution. It is the first structure of a member of homology family I.1 of bacterial lipases. The structure shows a variant of the α/β hydrolase fold, with Ser^{82}, Asp^{229}, and His^{251} as the catalytic triad residues. Compared with the "canonical" α/β hydrolase fold, the first two β-strands and one α-helix (αE) are not present. The absence of helix αE allows the formation of a stabilizing intramolecular disulfide bridge. The loop containing His^{251} is stabilized by an octahedrally coordinated calcium ion. On top of the active site a lid subdomain is in an open conformation, making the catalytic cleft accessible from the solvent region. A triacylglycerol analogue is covalently bound to Ser^{82} in the active site, demonstrating the position of the oxyanion hole and of the three pockets that accommodate the *sn*-1, *sn*-2, and *sn*-3 fatty acid chains. The inhibited enzyme can be thought to mimic the structure of the tetrahedral intermediate that occurs during the acylation step of the reaction. Analysis of the binding mode of the inhibitor suggests that the size of the acyl pocket and the size and interactions of the *sn*-2 binding pocket are the predominant determinants of the regio- and enantio-preference of the enzyme.

Lipases are triacylglycerol ester hydrolases (EC 3.1.1.3) that catalyze the hydrolysis of long chain acylglycerols. Since the beginning of the 1990s, the three-dimensional structures of an impressive number of lipases from mammalian, yeast, and microbial origin have been determined (1–3). In particular, structures of fungal and bacterial lipases have attracted interest because these enzymes are applied on a large scale in detergents and for stereoselective biotransformations. Their widespread biotechnological application is related to their cofactor independence, their broad substrate specificity, their high enantio-selectivity, and their stability in organic solvents (4).

Bacterial lipases have recently been classified into eight different families, with family I being the largest and consisting of six subfamilies (5). Families I.1 and I.2 contain lipases from the genus *Pseudomonas*. These lipases usually show pronounced differences in regio- and enantio-selectivity despite a high degree of amino acid sequence homology (more than 40%) (6, 7). They are widely used in industry, especially for the production of chiral chemicals that serve as basic building blocks in the synthesis of pharmaceuticals, pesticides, and insecticides (8).

The prototype enzyme of family I.1 is the 29-kDa extracellular lipase from *Pseudomonas aeruginosa*, which was the first *Pseudomonas* lipase to be purified to electrophoretic homogeneity (9). This enzyme has since been studied in great detail mainly because of the two following reasons. (i) It plays an important role as a virulence factor of *P. aeruginosa*, which is an opportunistic pathogen, causing a variety of infectious diseases in immuno-compromised patients. This lipase can act synergistically with other lipolytic enzymes, leading to damage of host cellular membrane lipids including lung surfactants (10). (ii) *P. aeruginosa* lipase is widely used for biotechnological applications because it is a versatile enzyme that can catalyze the hydrolysis and synthesis of a wide variety of industrially important substrates with broad specificity (4, 11–13).

Among *Pseudomonas* lipases only those belonging to family I.2 are known in atomic detail (5). These include the lipases from *Chromobacterium viscosum*, *Pseudomonas glumae*, and *Pseudomonas cepacia* (the latter two renamed *Burkholderia glumae* and *Burkholderia cepacia*) (14–17). The *C. viscosum* and *B. glumae* lipases are 100% identical in sequence, and their x-ray structures show the enzymes in a closed conformation, with an α-helical lid covering the active site and protecting it from the solvent phase (14, 15). In contrast, the *B. cepacia* lipase was crystallized in an open conformation, both in the absence and in the presence of a bound substrate-like inhibitor (16–19).

Here we report the x-ray structure of *P. aeruginosa* PAO1 lipase (PAL)[1] at 2.54 Å resolution, in the open conformation. The enzyme has been cocrystallized with the substrate ana-

* Financial support was obtained from European Union Eu-lipase Contract BI02-CT94-3013. The costs of publication of this article were defrayed in part by the payment of page charges. This article must therefore be hereby marked "*advertisement*" in accordance with 18 U.S.C. Section 1734 solely to indicate this fact.

The atomic coordinates and structure factors (code 1EX9) have been deposited in the Protein Data Bank, Research Collaboratory for Structural Bioinformatics, Rutgers University, New Brunswick, NJ (http://www.rcsb.org/).

§ Present address: Advanced Biotechnology Center, X-ray Structural Biology Laboratory, Largo Rosanna Benzi 10, 16132 Genova, Italy.

¶ These authors contributed equally to the work reported in this paper.

** Present address: Fresenius Medical Care Deutschland GmbH Medecine, Else-Kröner-Straβe 1, 61346 Bad Homburg, Germany.

§§ To whom correspondence should be addressed: Laboratory of Biophysical Chemistry, Dept. of Chemistry, University of Groningen, Nijenborgh 4, 9747 AG Groningen, The Netherlands. Fax: 31-50363-4800; E-mail: bauke@chem.rug.nl.

[1] The abbreviations used are: PAL, *P. aeruginosa* lipase; BGL, *B. glumae* lipase; CVL, *C. viscosum* lipase; BCL, *B. cepacia* lipase; R_C-trioctyl, R_C-(R_P,S_P)-1,2-dioctylcarbamoyl-glycero-3-*O*-*p*-nitrophenyl octylphosphonate.

TABLE I
Data collection and molecular replacement statistics

Data collection statistics	
Space group	$P2_12_12_1$
Cell dimensions	a = 146.62 Å, b = 100.20 Å, c = 96.88 Å
Resolution limit	2.54 Å
Observations	34,304
Unique reflections	8,772
Completeness (%) overall (outer shell)	98.3 (98.2)
R_{merge} [a] (%)(outer shell)	11.9 (33.6)
I/σ(I) (outer shell)	7.4 (4.2)
Molecular replacement	
Rotation (°)	α = 23.2 °, β = 30.5 °, γ = 348.9 °
Translation	x = 0.130, y = 0.003, z = 0.277
Correlation Coefficient/ R_{factor}	0.304/0.501

[a] $R_{merge} = \Sigma_h\Sigma_i \mid I_{hi} - \langle I_h \rangle \mid / \Sigma_h\Sigma_i I_{hi}$.

TABLE II
Refinement statistics

Refinement statistics	
Resolution range (Å)	25.0–2.54
R_{factor} [a]/R_{free} [b] (%)	19.3/23.7
Number of residues	285
Number of water molecules	112
Number of calcium ions	1
Number of inhibitor molecules	1
Root mean square deviation from ideality	
Bond lengths (Å)/bond angles (°)	0.012/1.530
Ramachandran plot	
Residues in most favored regions (%)	90.0
Residues in additional allowed regions (%)	9.6
Residues in disallowed regions (%)	0.4

[a] $R_{factor} = \Sigma_h \mid \mid F_{obs} \mid - \mid F_{calc} \mid \mid / \Sigma \mid F_{obs} \mid$, where F_{obs} and F_{calc} are the observed and calculated structure factor amplitudes, respectively.
[b] R_{free} is calculated with 5% of the diffraction data, which were not used during the refinement.

logue 1,2-dioctylcarbamoyl-glycero-3-*O*-*p*-nitrophenyl octylphosphonate, which binds covalently to the enzyme. The structure provides a structural description of the enzyme in its activated state and allows a detailed explanation of the regio- and stereoselectivity of the enzyme toward triglyceride substrates. These results can be generalized to other members of the bacterial lipase family I.1.

EXPERIMENTAL PROCEDURES

Crystallization and Data Collection—The lipase from *P. aeruginosa* was cloned, overexpressed, and purified as described previously (20). Crystallization of the inhibited enzyme was achieved by the sitting drop vapor diffusion method at room temperature. The protein solution, containing 5 mg/ml lipase, 10 mM Tris/HCl (pH 8.0), and 1% β-octylpyranoside, was incubated for 90 h at 12 °C in a 1:10 ratio with R_C-(R_P,S_P)-1,2-dioctylcarbamoyl-glycero-3-*O*-*p*-nitrophenyl octylphosphonate (R_C-trioctyl) (21). After incubation, the lipase-inhibitor complex was equilibrated against a precipitant solution containing 25% 2-methyl-2,4-pentanediol, 20 mM $CaCl_2$ in 100 mM citrate buffer (pH 5.6). Rod-shaped crystals, suitable for x-ray analysis, grew within months. They were highly x-ray-sensitive, and therefore the data collection was performed at cryo temperature (100 K), using the mother liquor as the cryoprotectant.

The crystals diffracted up to 2.54 Å resolution using synchrotron radiation. They belong to space group $P2_12_12_1$, with unit cell parameters of a = 45.47 Å, b = 50.96 Å, c = 110.02 Å. This unit cell gives a V_M value of 2.2 Å^3 Da^{-1} assuming 1 molecule of 29 kDa per asymmetric unit. A native data set was collected with a MAR Research image plate system at beamline BW7B of the EMBL Outstation at DESY, Hamburg. Data were integrated and merged using the DENZO/SCALEPACK package (22) and CCP4 software (23). Data processing statistics are given in Table I.

Structure Determination and Refinement—The structure was determined by molecular replacement using the program AMoRe (24) as implemented in the CCP4 program package (23). A homology model of *P. aeruginosa* lipase (12), built on the basis of its 42% sequence identity to *B. cepacia* lipase, of which a structure in the open conformation is known (Ref. 17; Protein Data Bank code 3LIP), was successfully used for a rotational search. The best result was obtained by including in the search model all the side chains. The rotational search clearly indicated a solution at α = 23.2°, β = 30.5°, γ = 348.9°, with a correlation coefficient of 0.185. A translational search performed using data in the 4–8-Å resolution range resulted in a solution at x = 0.130, y = 0.003, z = 0.277, with a correlation coefficient of 0.277 and an R_{factor} of 0.511. After rigid-body refinement of this solution, the final correlation coefficient and R_{factor} were 0.304 and 0.501, respectively (Table I). Despite the poor quality of the initial electron density map, the covalent bond present between the nucleophile (Ser^{82}) and the phosphonate inhibitor was perfectly visible as well as the *sn*-3 moiety of the triglyceride analogue. This was interpreted as a clear indication of the correctness of the molecular replacement solution. Many cycles of manual rebuilding, using the program O (25), and refinement, using the program CNS (26) (rigid body and simulated annealing at the beginning, conventional positional refinement and restrained individual B-factor refinement in the final stages), were necessary to improve the electron density map and to make the loops visible that in the initial maps were not visible at all. The best refinement results were obtained using a flat bulk solvent correction. Water molecules and a calcium ion were placed according to strict density and distance criteria.

Model Quality and Accuracy—The final model consists of 285 amino acid residues, one calcium ion, 112 water molecules, and one molecule of R_C-trioctyl (with the phosphorus atom in the S_P configuration) covalently bound to the catalytic Ser^{82}. All protein residues are visible in the electron density map as well as the *sn*-3 moiety of the inhibitor. For the *sn*-1 and *sn*-2 moieties, only discontinuous density is present, probably due to high mobility of these triglyceride chains, as reflected by their B-factors (55–68 Å^2). The crystallographic R_{factor} and R_{free} of the final model are 0.193 and 0.237, respectively. The stereochemical quality of the structure was assessed with the programs PROCHECK (27) and WHATCHECK (28). Only Ser^{82} is in a disallowed region of the Ramachandran plot (29), as expected for the nucleophile of a member of the α/β hydrolase fold family. Val^{258} is in a *cis*-peptide conformation. The structure was further analyzed using the program DALI (30). Refinement statistics are given in Table II. The atomic coordinates and the structure factors have been deposited to the Protein Data Bank with the entry code 1EX9.

RESULTS AND DISCUSSION

Overall Structure—P. aeruginosa lipase has a nearly globular shape with approximate dimensions of 35 × 40 × 50 Å^3. Its structure consists of a "core" domain (residues 1–108 and 164–285), showing the typical features of the α/β hydrolase fold topology (31–33), and a "cap" domain (residues 109–163), with four α-helices (α4, α5, α6, and α8) that shape the active site cleft (Fig. 1). Helix α5 and its neighboring loops can be considered as a "lid" in the open conformation, making the active site cavity accessible to solvent and substrate (Fig. 1*A*). Compared with the canonical α/β hydrolase fold (Fig. 1*B*), the first two β-strands are absent, and therefore, to be consistent with the numbering of the consensus α/β hydrolase fold, the first strand in the PAL structure is named β3. The helix corresponding to the canonical helix αE is absent too. Furthermore, an additional small antiparallel β-sheet (β-strands b1 and b2) is inserted between strand β3 and helix α1, and an additional β-strand (β'8) lines up with the sixth strand (β8) of the central β-sheet, but in the opposite direction (Fig. 1*B*).

P. aeruginosa lipase is the first member of family I.1 of bacterial lipases of which a crystal structure has been elucidated. Its structure is similar to the family I.2 lipase structures from *B. glumae* (BGL) (15), *B. cepacia* (BCL) (16–19), and *C. viscosum* (CVL) (14), which show 42% amino acid sequence identity to PAL. The structural similarity is mainly localized in the core domain, where the secondary structure elements correspond well (Figs. 2 and 3). Nevertheless, major differences occur in the region following strand β7, where in PAL a deletion of more than 20 residues results in the absence of the antiparallel β-sheet formed by strands b3 and b4 (Fig. 3). As a consequence, helix α8 of PAL superimposes on helix α9 of homology family I.2 lipases. Most importantly, helix α10 in

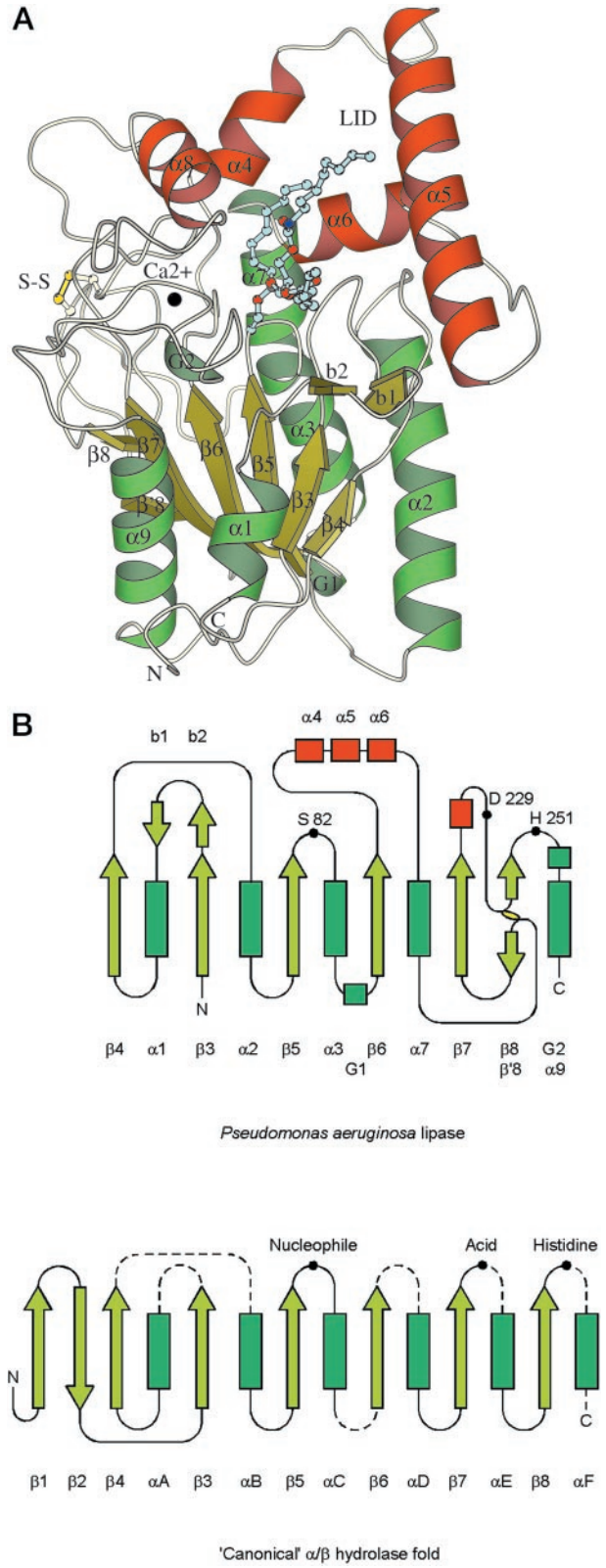

FIG. 1. **Structure of *P. aeruginosa* lipase.** *A*, schematic view of the secondary structure elements of PAL. The ribbon representation was made using MOLSCRIPT (35); α-helices, β-strands, and coils are represented by *helical ribbons*, *arrows*, and *ropes*, respectively. α-Helices belonging to the cap domain involved in substrate binding are shown in *red*. The position of the α-helical lid is highlighted with the label *LID*. The phosphonate inhibitor covalently bound to the nucleophile Ser^{82}, the calcium ion, and the disulfide bridge are in *ball* and *stick* representation in *cyan*, *black*, and *yellow*, respectively. *B*, secondary structure topology diagram of PAL. The catalytic triad residues (Ser^{82}, Asp^{229}, and His^{251}) and the position of the disulfide bridge are indicated, and a comparison with the canonical α/β hydrolase fold is given. α-Helices and β-strands are represented by *rectangles* and *arrows*, respectively. G1 and G2 are 3_{10} helices and are represented by *squares*. Locations where insertions in the canonical fold may occur are indicated by *dashed lines*.

homology family I.2 structures (equivalent to helix αE in the canonical α/β hydrolase fold) is absent in PAL (Fig. 1*B*), with the corresponding residues 234–237 classified as a "hydrogen-bonded turn" (27, 30). Residue Cys^{235} in this turn forms a disulfide bond with Cys^{183}, cross-linking the loops at the N-terminal sides of strands β8 and β′8 (Fig. 1). Although this disulfide bridge is conserved in BCL (Cys^{190}–Cys^{270}) and BGL/CVL (Cys^{190}–Cys^{269}) (Fig. 3), the PAL Cys^{183} does not superimpose well on the family I.2 Cys^{190} due to a three-residue deletion just after helix α7 in PAL. This deletion brings the PAL Cys^{183} Cα atom about 1.5–2.0 Å removed from the position of the Cys^{190} Cα atom in BCL and BGL/CVL. As a consequence, the position of Cys^{235} has shifted as well. The absence of an α-helical structure for residues 234–237 allows PAL to compensate for the three-residue deletion and to bring Cys^{235} at the correct distance to Cys^{183} for disulfide bridge formation. Mutation of both cysteine residues to serines rendered PAL more sensitive to heat denaturation and proteolytic degradation, suggesting a role of the disulfide bond in stabilizing the molecule (13).

It is interesting to notice that PAL Cys^{183} and Cys^{235} are highly but not absolutely conserved among the members of bacterial lipase family I.1 (Fig. 3). A disulfide bond interaction similar to PAL is likely to be present in *Vibrio cholerae*, *Acinetobacter calcoaceticus*, *Pseudomonas wisconsinensis*, and *Pseudomonas luteola* lipases. In contrast, the *Pseudomonas fragi*, *Phaseolus vulgaris*, and *Pseudomonas fluorescens* lipases lack this interaction. The first two enzymes have only one cysteine residue in their sequence, Cys^{75} and Cys^{88}, respectively, whereas *P. fluorescens* has two cysteines, Cys^{219} and Cys^{233}, but none of them matches the positions of the cysteine residues in PAL (Fig. 3).

Since the PAL structure is in the open conformation similar to BCL, whereas BGL and CVL are in a closed conformation (Fig. 2), a direct comparison of PAL and BCL can show the structural analogies and differences of the activated form of lipases from bacterial homology families I.1 and I.2. Fig. 2 shows that the three-dimensional similarity of PAL and BCL extends to the cap region. The two open structures superimpose with an root mean square difference of 1.12 Å for 264 structural equivalent Cα atoms out of 285 common Cα atoms. However, the α-helices α4, α5, and α6 of the cap subdomain do not superimpose perfectly in the two enzymes. Helix α5 is one turn longer in PAL than in BCL because of a three-residue insertion in PAL at the C terminus of the helix. The loop connecting α4 and α5 in PAL is three residues shorter than in BCL. Furthermore, helix α4 in PAL is shorter too and ends in a 3_{10} helical conformation (Fig. 3). Differences are also present in the location of helix α6, which in PAL immediately precedes helix α7, so much that helices α6 and α7 can be considered as one single α-helix with a bend of about 90° at the first residue of α7 (Ser^{164}).

Catalytic Triad—The catalytic triad residues Ser^{82} (nucleophile), Asp^{229} (acid), and His^{251} are located at their canonical positions in the α/β hydrolase fold (31). Their positions and orientations are similar to the catalytic triad residues in the family I.2 lipases. Ser^{82} is situated at the very sharp "nucleophile elbow" between strand β5 and helix α3, identified by the consensus sequence Gly-*X*-Ser-*X*-Gly (in PAL, *X* = His at both positions). As in all other α/β hydrolase-fold enzymes of which

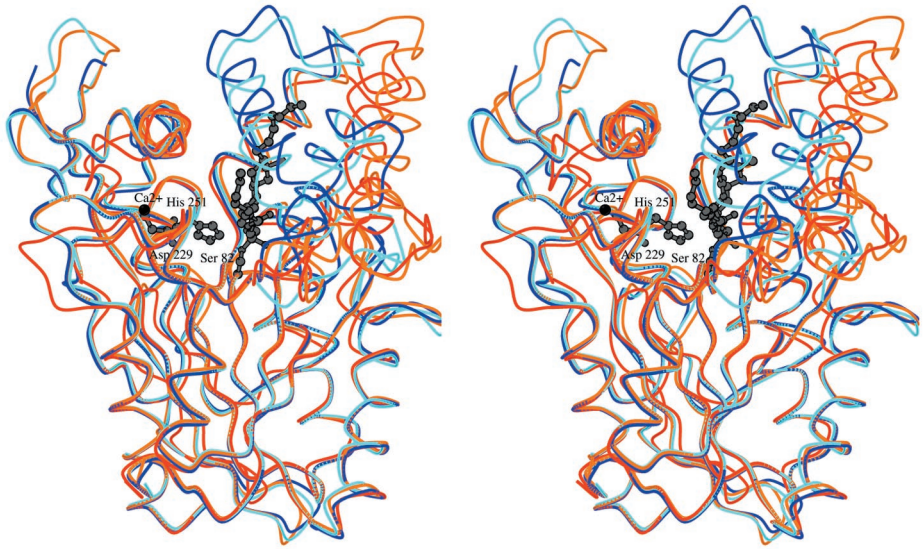

FIG. 2. **Stereo view of the superimposition of lipases from *P. aeruginosa*, *B. cepacia*, *B. glumae*, and *C. viscosum*.** PAL and BCL are in the open conformation and are shown in *red* and in *orange*, respectively. BGL and CVL are in the closed conformation and are shown in *blue* and *cyan*, respectively. The catalytic triad, with the R_C-trioctyl inhibitor (*gray*) covalently bound to the nucleophile, and the calcium ion (*black*) of PAL are shown in *ball* and *stick* representation. The lid of BGL and CVL overlaps the position where the inhibitor is localized in PAL. The figure was drawn using MOLSCRIPT (35).

the three-dimensional structure has been elucidated (33), the nucleophile adopts unfavorable torsion angles ($\phi = 57°$, $\psi = -111°$) and imposes steric restrictions on the residues located in its proximity. An intricate hydrogen-bonding pattern similar to that found in family I.2 lipases stabilizes the active site residues. The main chain nitrogen atom of Ser^{82} is hydrogen-bonded to the carbonyl oxygen atom of Val^{105}. The Ser^{82} side chain Oγ atom, covalently bound to the trioctyl inhibitor, is 3.0 Å from the catalytic histidine Nϵ2 atom, but the geometry is not suitable for a hydrogen bond between these two atoms. Instead, the His^{251} Nϵ2 makes a 2.8-Å hydrogen bond to the O1 of the phosphonate inhibitor (Fig. 4*B*). The His^{251} carbonyl oxygen and amide nitrogen atoms are hydrogen-bonded to the His^{81} Nϵ2 atom and Asp^{229} carbonyl oxygen atom, respectively. Most importantly, the His^{251} Nδ1 is 3.1 Å from the Oδ2 of the Asp^{229} side chain that is responsible for stabilizing the positively charged His^{251} side chain during catalysis. The Asp^{229} Oδ2 atom is not only at hydrogen-bonding distance from the catalytic histidine but is also very close (2.7 Å) to the Glu^{254} Oϵ2 atom. The Glu^{254} Oϵ1 atom is 3.6 Å away from the His^{251} Nδ1 atom and, therefore, does not interact directly with the triad histidine. However, it has been suggested for *B. glumae* lipase (15) that an acid residue at that position may assist the catalytic histidine during hydrolysis, either directly or via a water molecule, if the triad acid (Asp/Glu) is mutated. This could also be the case for the *P. aeruginosa* lipase.

Ca^{2+}-binding Site—Approximately 15 Å from the nucleophile Ser^{82}, at the same side of the enzyme where the catalytic His^{251} is located, a calcium binding pocket is present. The calcium ion is octahedrally coordinated, and its ligands are the two carboxylate groups of Asp^{209} and Asp^{253} (both absolutely conserved in all family I.1 and I.2 lipases), the two carbonyl oxygen atoms of Gln^{257} and Leu^{261}, and two water molecules (Fig. 5). All the distances to calcium are within ~2.2–2.4 Å, and the low B_{factor} values of the ion and its ligands (17–30 $Å^2$) reflect a relatively rigid conformation of the calcium binding region. Despite the medium resolution (2.54 Å) of the PAL crystal structure, Val^{258} is unambiguously in a *cis*-peptide conformation. The *cis*-peptide bond between Gln^{257} and Val^{258} is stabilized by a conserved hydrogen-bonding network that extends to the catalytic His^{251}. The Ca^{2+} ion bridges helix α8, which forms part of the wall of the active site cleft, to the loop containing the catalytic histidine and, therefore, contributes to keep His^{251} at the correct position in the active site. The binding mode of the Ca^{2+} ion is conserved in BCL, BGL, and CVL, including the presence of a *cis*-peptide bond corresponding to Val^{258} in PAL. Furthermore, a structure-based sequence alignment of the bacterial lipases from families I.1 and I.2 shows the conservation of an Asn/Asp residue at the position preceding the catalytic histidine (Fig. 3). This Asn/Asp residue hydrogen bonds one of the two water molecules that coordinate the calcium ion. The other residues in PAL that interact with these water molecules (Thr^{205}, Ser^{211}, and Asp^{212}) are also highly conserved, with some variation that is not likely to influence the calcium binding. This can be deduced, for instance, from the fact that in the BCL, BGL, and CVL structures an alanine replaces PAL Thr^{205}, with the calcium-coordinating water molecule hydrogen bonded to another solvent molecule located at a position equivalent to the Thr^{205} Oγ1 atom in PAL.

Active Site Cleft and Inhibitor Binding—The PAL structure provides a rare example of a lipase complexed with a triglyceride-like inhibitor. The only other example is that of the family I.2 lipase from *B. cepacia*. Structural analysis of the open conformation of PAL and BCL in complex with the same R_C-trioctyl inhibitor (Fig. 4*A*) (21) offers the opportunity of a direct comparison of the binding mode of the substrate analogue in lipases from families I.1 and I.2.

In both PAL- and BCL-inhibited structures the R_C-trioctyl molecule is covalently linked at its phosphorus atom to the nucleophilic Oγ atom of the catalytic serine residue and perfectly fits into similar hydrophobic active site clefts. In PAL this cleft is 15 Å deep and has an ovoid shape with approximate dimensions of 10 × 25 Å. It is bordered by helices α4, α5, α8 and by the loops of residues 16 to 29 and 255 to 259. Its walls are lined mostly with hydrophobic side chains, making it perfectly suited for lipid binding. At the base of the cleft the Met^{16} side chain divides it in two parts, thus giving a characteristic boomerang-like shape to the active site, with four binding pockets, an oxyanion hole and three pockets for the different branches of the triacylglycerol substrate (Fig. 4*B*).

In PAL the Met^{16} and His^{83} main chain amide groups are 2.8 Å and 2.9 Å from one of the phosphorous oxygen atoms (O4) (Fig. 4*B*). A similar interaction is present in BCL involving Leu^{17} and Gln^{88} residues. Since the R_C-trioctyl-complexed structure represents the putative tetrahedral intermediate conformation during the acylation step of the reaction, the Met^{16} and His^{83} backbone nitrogen atoms localize the oxyanion binding pocket in a position very well conserved within the α/β hydrolase-fold enzymes (31, 33, 34). Met^{16} is the second residue of the tetrapeptide motif Gly-Hyd-*X*-Gly (Hyd = Met, Leu, Val) located between strand β3 and helix α4 and highly conserved in families I.1 and I.2 of bacterial lipases (Fig. 3). In PAL this

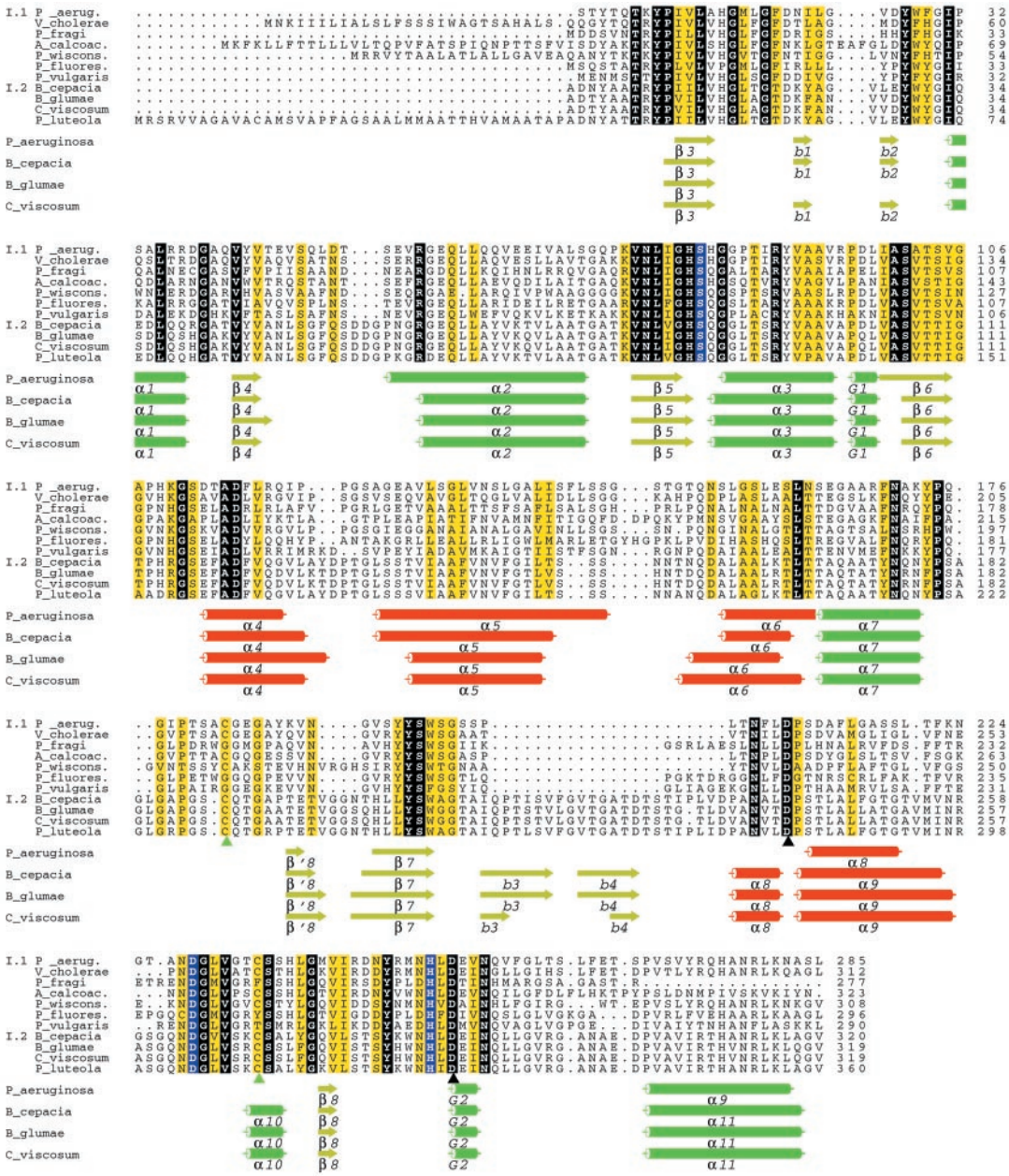

FIG. 3. **Structure-based sequence alignment of bacterial lipases from homology family I.1 and I.2.** The comparison of the amino acid sequences of bacterial lipases from homology family I.1 (*P. aeruginosa*, *V. cholerae*, *P. fragi*, *A. calcoaceticus*, *P. wisconsinensis*, *P. fluorescens*, and *P. vulgaris*) and from homology family I.2 (*B. cepacia*, *B. glumae*, *C. viscosum*, and *P. luteola*) has been performed using the program CLUSTALW (36) and manually inspected and corrected on the basis of the three-dimensional structure comparison of PAL, BCL, BGL, and CVL. *Shaded regions* indicate the catalytic triad residues (*blue*) and identical (*black*) or similar (*yellow*) amino acids in all the aligned sequences. The two Asp residues that coordinate the calcium ion and the two Cys residues that make a disulfide bridge are highlighted by *black* and *green triangles*, respectively. α-Helices and β-strands are represented by *rectangles* and *arrows*, respectively. G1 and G2 are 3_{10} helices. The color code of secondary structure elements is in accordance to Fig. 1. The figure has been prepared with ALSCRIPT (37).

tetrapeptide motif is stabilized by a hydrogen bond between the His^{14} carbonyl oxygen atom and the Arg^{56} NH_2 atom. Arg^{56} is a totally buried residue that lies at the beginning of helix $\alpha 2$, close to the nucleophile elbow. It connects the oxyanion hole tetrapeptide motif to the loop between strand $\beta 3$ and helix $\alpha 2$ via the hydrogen bond Arg^{56} NH1-Ser^{48} O. Interestingly, Arg^{56} is totally conserved in homology family I.1 as well as in homology family I.2 lipases (Fig. 3). In the open conformation of BCL the interaction pattern of this Arg (Arg^{61}) strongly resembles that of PAL Arg^{56}, with the Arg^{61} side chain hydrogen-bonded to the carbonyl oxygen atom of His^{15} and Ser^{50}. In contrast, in the closed conformations of CVL and BGL, the Arg^{61} side chain is hydrogen-bonded to the carbonyl oxygen atoms of Leu^{17} and Gly^{51} and of Gly^{16} and Phe^{52}, respectively. Since the movements of the loop between strand $\beta 4$ and helix $\alpha 2$ (PAL residues 45–52), of the oxyanion loop (PAL residues 14–20), and of the lid region are correlated (17), the variation of the hydrogen-bonding pattern of this conserved Arg residue might play an important stabilizing role during the opening of the lid of these lipases.

In PAL the *sn*-3 octyl chain of the inhibitor (atoms C4-C11) is accommodated in a large groove (about 8.5 Å × 9.0 Å) formed by the side chains of Met^{16}, Pro^{108}, Ser^{112}, Thr^{114}, Ala^{115}, Leu^{118}, Leu^{131}, Val^{135}, Leu^{159}, Leu^{162}, Leu^{231}, and Val^{232} (acyl chain pocket HA). The octyl group of the inhibitor fits snugly in this cleft and is bound via van der Waals interactions. Because of its size, the acyl binding pocket may easily accommodate up to about 12 fatty acid carbon atoms. The binding of the *sn*-3

moiety in the acyl-binding pocket (HA) is almost identical in PAL and BCL.

The alcohol binding pocket is separated from the acyl pocket by the side chain of Met[16] and contains the bound lipid analogue in a bent "tuning fork" conformation (Fig. 4*B*). The *sn*-2 moiety (atoms N2-C30) fits in a hydrophobic pocket lined by Leu[17], Phe[19], Ile[22], Val[25], Tyr[27], Leu[252], Val[255], Gln[257], Val[258], and Phe[259] (HH pocket). The latter residues are part of the calcium binding loop (residues 252 to 261). The HH pocket is slightly larger in PAL compared with that of BCL, and consequently, the enzyme-inhibitor interactions are less tight than in BCL. There is space for about 8–10 fatty acid carbon atoms to be accommodated in this pocket. Longer chains would partly stick into the solvent or micelle. In the HH pocket all the enzyme-inhibitor interactions are hydrophobic, and the NH group of the carbamoyl function of this chain does not have any specific hydrogen-bonding interactions with the protein. In particular, the hydrogen bond which in BCL connects the Thr[18] Oγ atom to the carbonyl oxygen of the carbamoyl function of the *sn*-2 chain is absent in PAL due to the presence of a hydrophobic residue, Leu[17], instead of the polar Thr[18] in BCL.

The *sn-1* inhibitor moiety (atoms N1-C20) interacts less tightly with the enzyme than the *sn*-2 chain. It is located in a pocket more exposed to the solvent (HB pocket). The only specific interactions with the protein are van der Waals contacts with the side chains of Leu[17], Leu[138], and Phe[214]. The location of the *sn*-1 chain is mainly determined by a hydrophobic clamp formed by Phe[214] and Leu[138]. The *sn*-1 chain diverges considerably with respect to the position found in the BCL complex since in the latter lipase the bulky side chain of Phe[214] is substituted for an Ala[247] (Fig. 3). As for the *sn*-2 moiety, the *sn*-1 NH group of the carbamoyl function does not specifically interact with the protein. Pro[210] and Ser[211] are located between the two *sn*-1 and *sn*-2 moieties but too far away to make any direct interaction. Since the HH pocket hosting the *sn*-2 chain provides a more intimate interaction with the substrate analogue than the HB pocket occupied by the *sn*-1 chain, the HH pocket is most likely the one that determines the regio-preference of the enzyme toward the primary position of triglyceride substrates together with the size of the acyl chain pocket HA.

In view of the differences in the inhibitor binding modes in the alcohol binding pocket, it is not surprising that PAL and BCL differ somewhat in their stereospecificity. BCL prefers the R_C-trioctyl inhibitor over the S_C-trioctyl compound by a factor of 7. It has been suggested that Leu[287] and Ile[290] play an important role in conferring this preference by providing unfavorable interactions with the carbonyl oxygen (O7) of the S_C-trioctyl compound (18). Furthermore, the hydrophilic interaction of the *sn*-2 carbonyl oxygen (O6) with the Oγ1 atom of Thr[18] favors this preference (18). In contrast, in PAL the residue corresponding to BCL Ile[290] is Val[255], a less bulky residue, and BCL Thr[18] corresponds to Leu[17] in PAL, a non-polar residue (Fig. 3). These differences explain why PAL prefers the R_C-trioctyl inhibitor only by a factor of 1.5 over the S_C-trioctyl compound.[2]

Conclusions—The x-ray structure of *P. aeruginosa* lipase provides the first three-dimensional structure of a member of homology family I.1 of bacterial lipases. The molecule is in the open conformation and the active site contains a triacylglycerol analogue covalently bound to the catalytic nucleophile, Ser[82]. The other catalytic residues are Asp[229] and His[251]. An octahedrally coordinated calcium ion stabilizes the loop containing the catalytic histidine. Sequence alignment with other lipases of homology family I.1 shows that the residues important for catalysis and fold stabilization are conserved.

The bound inhibitor unambigously identifies the position of the oxyanion hole and the three pockets that accommodate the *sn*-1, *sn*-2, and *sn*-3 fatty acid chains, thus providing a picture of the tetrahedral intermediate that occurs during the acylation step of the triacylglycerol hydrolysis reaction. At the base of the active site cleft the Met[16] side chain divides the cleft into two branches, thus creating the acyl pocket for the binding of the *sn*-3 moiety of the inhibitor on one side and the alcohol pocket for the binding

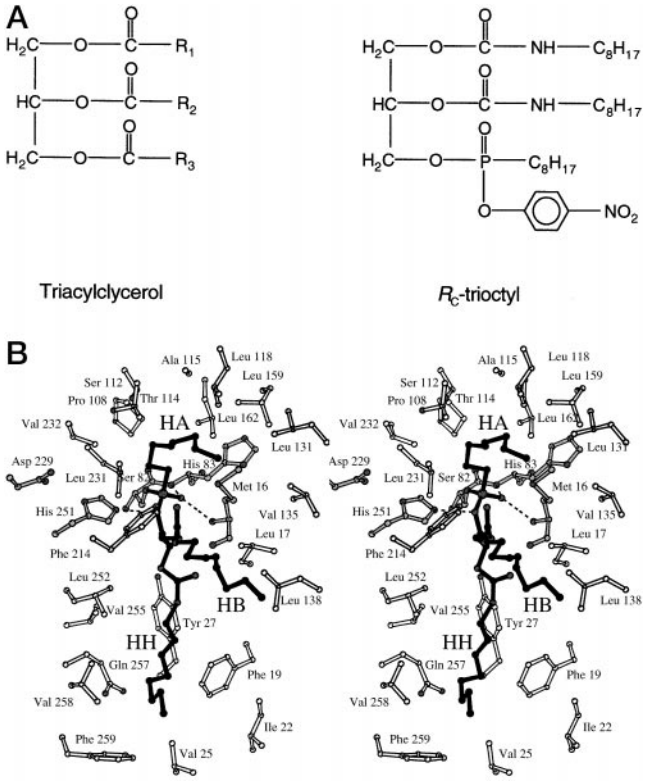

FIG. 4. **Binding of the R_C-trioctyl inhibitor to *P. aeruginosa* lipase.** *A*, schematic representation of the phosphonate inhibitor in comparison with a triacylglycerol molecule. *B*, stereo view of the binding mode of R_C-trioctyl in PAL active site. The inhibitor (*black*), the catalytic triad (*gray*), the oxyanion hole residues (*gray*), and the residues that line the three acyl chain binding pockets (HA, HB, HH) (*white*) are in *ball* and *stick* representation. Hydrogen bonds are shown by *dashed lines.* The figure was produced using MOLSCRIPT (35).

[2] K. Liebeton and K.-E. Jaeger, manuscript in preparation.

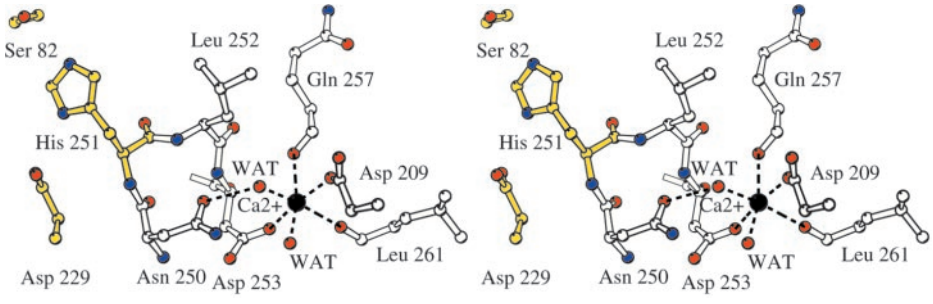

FIG. 5. **Ca^{2+}-binding site.** Stereo view of PAL calcium binding site. The catalytic triad (*yellow*) and the residues and water molecules that coordinate the calcium ion (*black*) are in *ball* and *stick* representation. The octahedral coordination of the Ca^{2+} ion is shown by *dashed lines*. The figure was drawn using MOLSCRIPT (35).

of the *sn*-1 and *sn*-2 chains on the other side. The interactions between inhibitor and enzyme are mostly of a hydrophobic nature. Since the pocket hosting the *sn*-2 chain provides a more intimate interaction with the substrate analogue than the one occupied by the *sn*-1 chain, the *sn*-2 binding pocket and the acyl chain pocket are the ones that predominantly determine the regio-preference of the enzyme. Furthermore, comparison of PAL and *B. cepacia* lipase, both in complex with R_C-trioctyl, suggests Val^{255} and Leu^{17} to play a role in the differences in enantiospecificity of the enzymes toward the triacylglycerol analogue. These results pave the way for site-directed mutagenesis experiments to improve the enzyme for application in bioconversion reactions.

Acknowledgments—We thank Birgit Forth and Susanne Tetling for purification of PAL and M. Mannesse for supplying the phosphonate inhibitor.

REFERENCES

1. Borgström B., and Brockman, H. L. (1984) *Lipases*, Elsevier Science Publishers B.V., Amsterdam
2. Schrag, J. D., and Cygler, M. (1997) *Methods Enzymol.* **284,** 85–107
3. Jaeger, K.-E., Ransac, S., Dijkstra, B. W., Colson, C., van Heuvel, M., and Misset, O. (1994) *FEMS Microbiol. Rev.* **15,** 29–63
4. Jaeger, K.-E., and Reetz, M. T. (1998) *Trends Biotechnol.* **16,** 396–403
5. Arpigny J. L., and Jaeger K.-E. (1999) *Biochem. J.* **343,** 177–183
6. Gilbert, E. J. (1993) *Enzyme Microb. Technol.* **15,** 634–645
7. Svendsen A., Borch, K., Barfoed, M., Nielsen, T. B., Gormsen, E., and Patkar, S. A. (1995) *Biochim. Biophys. Acta* **1259,** 9–17
8. Theil, F. (1995) *Chem. Rev.* **95,** 2203–2227
9. Stuer, W., Jaeger, K.-E., and Winkler, U. K. (1986) *J. Bacteriol.* **168,** 1070–1074
10. Jaeger, K.-E. (1994) *Immun. Infekt.* **22,** 177–180
11. Kazlauskas, R. J., and Weber, H. K. (1998) *Curr. Opin. Chem. Biol.* **2,** 121–126
12. Jaeger, K.-E., Schneidinger, B., Rosenau, F., Werner, M., Lang, D., Dijkstra, B. W., Schimossek, K., Zonta, A., and Reetz, M. T. (1997) *J. Mol. Catal. B* **3,** 3–12
13. Jaeger, K.-E., Dijkstra, B. W., and Reetz, M. T. (1999) *Annu. Rev. Microbiol.* **53,** 315–351
14. Lang, D., Hofmann, B., Haalck, L., Hecht, H.-J., Spener, F., Schmid, R. D., and Schomburg, D. (1996) *J. Mol. Biol.* **259,** 704–717
15. Noble, M. E. M., Cleasby, A., Johnson, L. N., Egmond, M. R., and Frenken, L. G. J. (1993) *FEBS Lett.* **331,** 123–128
16. Kim, K. K., Song, H. K., Shin, D. H., Hwang, K. Y., and Suh, S. W. (1997) *Structure* (*Lond.*) **5,** 173–185
17. Schrag, J. D., Li, Y., Cygler, M., Lang, D., Burgdorf, T., Hecht, H.-J., Schmid, R., Schomburg, D., Rydel, T. J., Oliver, J. D., Strickland, L. C., Dunaway, C. M., Larson, S. B., Day, J., and McPherson, A. (1997) *Structure* (*Lond.*) **5,** 187–202
18. Lang, D. A., Mannesse, M. L. M., De Haas, G. H., Verheij, H. M., and Dijkstra, B. W. (1998) *Eur. J. Biochem.* **254,** 333–340
19. Lang, D. A., and Dijkstra, B. W. (1998) *Chem. Phys. Lipids* **93,** 115–122
20. Jaeger, K.-E., Adrain, F.-J., Meyer, H. E., Hancock, R. E. W., and Winkler, U. K. (1992) *Biochim. Biophys. Acta* **1120,** 315–321
21. Mannesse, M. L. M., Boots, J. W. P., Dijkman, R., Slotboom, A. J., Vanderhijden, H. T. W. V., Egmond, M. R., Verheij, H. M., and de Haas, G. H. (1995) *Biochim. Biophys. Acta* **1259,** 56–64
22. Otwinowski, Z., and Minor, W. (1997) *Methods Enzymol.* **276,** 307–326
23. Collaborative Computational Project Number 4 (1994) *Acta Crystallogr. Sect. D* **50,** 760–763
24. Navaza, J. (1994) *Acta Crystallogr. Sect.* **50,** 157–163
25. Jones, T. A., Zou, J. Y., Cowan, S. W., and Kjeldgaard, M. (1991) *Acta Crystallogr. Sect. A* **47,** 110–119
26. Brünger, A. T., Adams, P. D., Clore, G. M., DeLano, W. L., Gros, P., Grosse-Kunstleve, R. W., Jiang, J.-S., Kuszewski, J., Nilges, M., Pannu, N. S., Read, R. J., Rice, L. M., Simonson, T., and Warren, G. L. (1998) *Acta Crystallogr. Sect. D* **54,** 905–921
27. Laskowski, R. A., MacArthur, M. W., Moss, D. S., and Thornton, J. M. (1993) *J. Appl. Crystallogr.* **26,** 283–291
28. Hooft, R. W. W., Vriend, G., Sander, C., and Abola, E. E. (1996) *Nature* **381,** 272
29. Ramakrishnan, C., and Ramachandran, G. N. (1965) *J. Mol. Biol.* **7,** 95–99
30. Holm, L., and Sander, C. (1994) *Proteins* **3,** 165–173
31. Ollis, D. L., Cheah, E., Cygler, M., Dijkstra, B., Frolow, F., Franken, S. M., Harel, M., Remington, S. J., Silman, I., Schrag, J., Sussman, J. L., Verschueren, K. H. G., and Goldman, A. (1992) *Protein Eng.* **5,** 197–211
32. Heikinheimo, P., Goldman, A., Jeffries, C., and Ollis, D. L. (1999) *Structure* (*Lond.*)**7,** 141–146
33. Nardini, M., and Dijkstra, B. W. (1999) *Curr. Opin. Struct. Biol.* **9,** 732–737
34. Cygler, M., and Schrag, J. D. (1997) *Methods Enzymol.* **284,** 3–27
35. Kraulis, P. (1991) *J. Appl. Crystallogr.* **24,** 946–950
36. Thompson, J. D., Higgins, D. G., and Gibson, T. J. (1994) *Nucleic Acids Res.* **22,** 4673–4680
37. Barton, G. J. (1993) *Protein Eng.* **6,** 37–40